

Advanced Scheduling Strategies for Distributed Quantum Computing Jobs

Gongyu Ni¹, Davide Ferrari², Lester Ho¹, and Michele Amoretti^{2,*}

¹*Wireless Communications Laboratory, Tyndall National Institute, Dublin, Ireland*

²*Quantum Software Laboratory, Department of Engineering and Architecture, University of Parma, Parma, 43124 Italy*
(<https://www.qslab.unipr.it/>)

*Corresponding author: Michele Amoretti, michele.amoretti@unipr.it.

Abstract

Distributed quantum computing (DQC) is being actively investigated as a means of scaling the number of qubits across multiple connected quantum devices. This includes quantum circuit compilation and execution management on multiple quantum devices in the network. The latter aspect is very challenging because, while reducing the makespan of job batches remains a relevant objective, novel quantum-specific constraints must be considered, including QPU utilization, non-local gate rate, and the latency associated with queued DQC jobs. In this work, a range of scheduling strategies is proposed, simulated, and evaluated, including heuristics that prioritize resource maximization for QPU utilization, node selection based on heterogeneous network connectivity, asynchronous node release upon job completion, and a scheduling strategy based on reinforcement learning with proximal policy optimization. These approaches are benchmarked against traditional FIFO and LIST schedulers under varying DQC job types and network conditions for the allocation of DQC jobs to devices within a network.

Index terms— Distributed quantum computing, Quantum network, Job Scheduling, Makespan, QPU utilization, Non-local gate rate

1 Introduction

Distributed quantum computing (DQC) scales the qubit capacity of quantum systems by interconnecting multiple QPUs and enabling collaborative computation. Unlike classical distributed computing, where scaling is typically linear, interconnecting quantum processors yields an exponential increase in computational power [1]. Achieving the DQC paradigm relies on a quantum network infrastructure to cluster multiple quantum processors and effectively increase the available number of

qubits. Communication between remote quantum processors requires the distribution and consumption of EPR pairs over quantum links before any inter-processor operations can be executed. EPR pairs, also denoted as Bell states, are the maximally entangled quantum states of a two-qubit system (i.e., a quantum mechanical system composed of two interacting two-level subsystems) [2, 3].

Transitioning from monolithic to distributed quantum computing introduces challenges in algorithm partitioning and execution management [4]. A quantum compiler is responsible for partitioning a monolithic algorithm into local and remote operations, as in [5, 6, 7]. Execution management, in contrast, focuses on scheduling distributed quantum circuit instances, or jobs, onto the quantum network for each execution round [8, 9, 10].

This paper focuses on the execution management of DQC jobs. In classical high performance computing, there is a rich literature of algorithms that aim to reduce the makespan of job batches while maximizing the utilization of computational resources [11, 12, 13]. In the DQC domain, execution management is much more challenging because, while reducing the makespan is still a relevant objective, novel quantum-specific constraints must be taken into account. These constraints are mostly related to the generation and distribution of EPR pairs: there is a tradeoff between rate and fidelity (which measures the quality of a quantum state). Furthermore, there is a time limit for consuming an entangled state before decoherence (i.e., loss of quantum information) due to interactions with the environment.

The main contributions of this paper lie in the definition, simulation, and evaluation of scheduling strategies for allocating DQC jobs to networked QPUs. An integrated simulation framework for distributed quantum computation jobs and their execution management is developed. Multiple scheduling strategies, including classical approaches (EPR, ASAP, and Resource-Prioritize) and a reinforcement learning-based PPO scheduler, are proposed and systematically evaluated under varying

DQC job types and network conditions.

The paper is organized as follows. In Section 2, related research on scheduling distributed computation tasks in quantum networks and classical distributed systems is reviewed. Section 3 presents the DQC workflow, including the quantum circuit compilation into multiple DQC jobs, the scheduling process, scheduler performance evaluation, and the network model comprising the description of the network topology and time-slot synchronization simulation. In Section 4, the performance metrics used to evaluate scheduling methods are introduced. In Section 5, multiple scheduling methods for distributing DQC jobs are explained in detail. In Section 6, the simulation settings and the analysis of the results are presented. Finally, Section 7 provides the conclusions of the paper.

2 Related Work

In classical distributed computing, scheduling multiple jobs concurrently is an NP-hard problem, including the optimization of the preemptive makespan [11]. Evaluations of distributed computing systems typically consider the execution time of individual and average jobs, as well as fairness across tasks [14].

In distributed quantum computing, both quantum and network operations should be considered. A monolithic quantum circuit is decomposed into multiple sub-circuits, with quantum and classical communication happening between them. These communicating sub-circuits constitute a DQC job, and designing effective management and scheduling strategies for DQC jobs remains an active area of research.

To minimize the total time consumed by quantum and network operations in DQC, the authors of [15] compare and contrast two approaches: a resource-constrained project scheduling (RCPSP) framework with batching and a greedy heuristic algorithm. At each time step, the RCPSP method evaluates which operations are eligible for scheduling based on the availability of quantum resources, such as communication and memory qubits, in order to optimize overall scheduling efficiency.

In [9], the authors distribute an accelerated variational quantum eigensolver (VQE) and propose a distributed quantum control system to manage resource allocation for executing quantum algorithms. In [10], the authors present a mathematical framework for parallel and distributed quantum algorithms and introduce a scheduling approach for programs running on networks of distributed quantum processors. Within this framework, they analyze three quantum algorithms.

Regarding parallelized DQC job scheduling, authors in [16] propose a scheduling algorithm that parallelizes quantum circuits with varying lengths and shot counts while mitigating parallel slowdowns caused by measurement synchronization. In [8], the authors also formulate

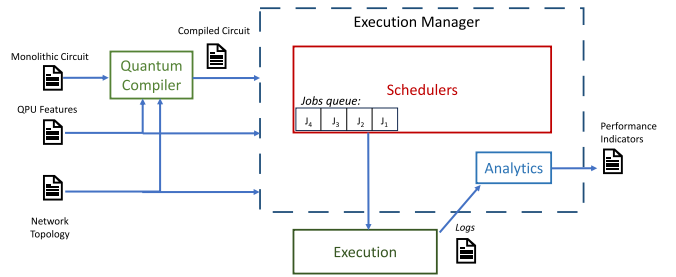


Figure 1: The DQC workflow decomposes a monolithic quantum circuit into sub-circuits (jobs). The execution manager synchronizes multiple schedulers, each independently allocating jobs across the network. The jobs are then executed, and the resulting simulation data are analyzed to assess the performance of each scheduler.

the scheduling task as a parallel job-scheduling problem, where a set of jobs with varying processing times must be assigned to multiple quantum processors. By estimating DQC job execution times using circuit depth (i.e., the number of layers), they propose parallelized FIFO and list-scheduling heuristics and evaluate their performance in terms of makespan, quantum-processor utilization, and network utilization.

3 DQC Framework

In this section, the DQC workflow and network model, including network link settings and synchronized network simulation, are presented.

3.1 DQC Workflow

The DQC workflow encompasses circuit compilation, decomposition of a monolithic quantum circuit into sub-circuits (each treated as an independent job), and allocation of Quantum Processing Unit (QPU) nodes to execute these jobs, as illustrated in Figure 1.

In Figure 1, the Quantum Compiler, as mentioned in [5], is applied to partition the circuit into executable sub-circuits based on the network topology and QPU capabilities, ensuring that inter-node dependencies are minimized. In contrast, the Scheduler manages the execution of these jobs by organizing the job queue and determining whether they should be executed concurrently or sequentially to achieve optimal performance and resource utilization.

In this work, we consider a fully connected QPU network topology, as it reduces the number of required non-local operations. Each QPU is equipped with data qubits and communication qubits and is treated as a node in the network. Links between nodes are heterogeneous, as indicated by the different colors in Figure 2.

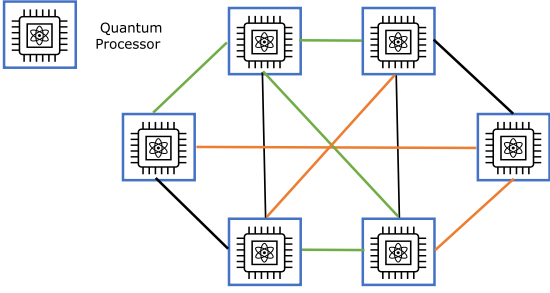


Figure 2: Fully connected QPU network with heterogeneous links.

3.2 Network Model

In the network model, heterogeneous links represent variations in the characteristics of the connections between nodes. Among different scheduling strategies for assigning DQC jobs to available network nodes, the synchronization of arriving jobs within each time slot is also considered.

3.2.1 Heterogeneous links

Links between nodes are characterized by several key parameters, including the entanglement generation cycle time, expected state delay, entanglement success probability, and fidelity. Each of them has an impact on the performance of DQC job execution.

In [17], the entanglement success probability P_s represents the probability that a single entanglement generation attempt succeeds. For a link of length d , it can be modeled as

$$P_s(d) = \frac{1}{2} \eta_{\text{penalty}} (\eta_{\text{ion}} \eta_{FC}^{\text{ion} \rightarrow \text{telecom}} \eta_{\text{det}}^{\text{telecom}})^2 10^{-(\alpha/10)(d/2)}, \quad (1)$$

where η_{ion} is the efficiency for emitting and collecting a photon, $\eta_{FC}^{\text{ion} \rightarrow \text{telecom}}$ is the efficiency of frequency conversion from ion to photons, $\eta_{\text{det}}^{\text{telecom}}$ is the detector efficiency for photons at telecom frequency, α is the attenuation factor, and η_{penalty} accounts for a penalty to truncate the detection window.

The cycle time t_{cycle} represents the average duration required for a single entanglement generation attempt. Shorter cycle times enable higher repetition rates and, thus, faster entanglement generation.

The state delay t_{state} represents the expected time to successfully generate an entangled state in a deterministic model and is given by

$$t_{\text{state}} = \frac{t_{\text{cycle}}}{P_s}. \quad (2)$$

Eq. (2) combines both the time for the entanglement generation attempt and the success probability to quantify the time needed to obtain a usable entangled state.

3.2.2 Synchronized Network Simulation

The simulation consists of multiple time slots. In each slot, jobs arrive randomly but remain consistent across different schedulers. The number of arriving jobs follows a truncated Poisson distribution with specified lower and upper bounds. Schedulers immediately receive jobs upon completing the previous queue, allowing the simulation to track execution times and latencies for individual jobs. This setup captures both the stochastic nature of job arrivals and the dynamic resource allocation across the network, enabling a comprehensive evaluation of DQC job scheduling and execution.

4 Performance Metrics

The performance metrics described in this section are used to evaluate the DQC job schedulers. Makespan indicates the total time consumed to execute an entire queue of DQC jobs, reflecting how efficiently all jobs are completed. QPU utilization and non-local gate rate measure how effectively the system uses local quantum resources (data qubits) and quantum network resources (EPR pairs). For overall system assessment, execution-latency performance and fairness metrics are also considered to evaluate both latency and fairness among jobs within the queue.

4.1 Makespan

The makespan M represents the total completion time of a queue of DQC jobs, defined as

$$M = \max_j (t_j^f) - \min_j (t_j^s), \quad (3)$$

where t_j^s and t_j^f denote the start and finish times of the j -th job, respectively. A shorter makespan indicates that the scheduler completes the DQC jobs more efficiently.

4.2 QPU Utilization

The QPU utilization [8] measures the proportion of QPU resources occupied by DQC jobs, normalized by the product of the makespan and the total number of available QPUs.

$$U_{\text{QPU}} = \frac{\sum_j p_j q_j}{M n_{\text{QPU}}} \in [0, 1], \quad (4)$$

where p_j is the execution time of job j , q_j is the number of QPUs required by that job, n_{QPU} is the total number of QPUs in the system, and M is the makespan. A higher QPUs utilization indicates that the scheduler uses most of the QPUs in the network, which is a desirable feature.

4.3 QPU Utilization

The QPU utilization [8] measures the proportion of QPU resources occupied by DQC jobs, normalized by the

product of the makespan and the total number of available QPUs.

$$U_{\text{QPU}} = \frac{\sum_j p_j q_j}{M n_{\text{QPU}}} \in [0, 1], \quad (5)$$

where p_j is the execution time of job j , q_j is the number of QPUs required by that job, n_{QPU} is the total number of QPUs in the system, and M is the makespan. A higher QPUs utilization indicates that the scheduler uses most of the QPUs in the network, which is a desirable feature.

4.4 Non-Local Gate Density

Non-local gate rate quantifies the non-local gates utilization rate for an incoming DQC job queue. For each job, the execution time includes both local and non-local quantum gates. Since non-local gates dominate the execution time, we approximate the overlap of non-local gate execution using the job execution time.

Let \mathcal{J} denote the arrival set of jobs, where each job $j \in \mathcal{J}$ has a start time t_j^s and a finish time t_j^f . Indices j and k represent two distinct jobs in \mathcal{J} .

The total pairwise overlapping time is defined as

$$T_{\text{overlap}} = \sum_{\substack{j,k \in \mathcal{J} \\ j < k}} \max(0, \min(t_j^f, t_k^f) - \max(t_j^s, t_k^s)), \quad (6)$$

where $j < k$ ensures that each job pair is counted once.

To normalize the pairwise overlapping time, we define the maximum possible overlap between every pair of jobs as

$$T_{\text{max}} = \sum_{\substack{j,k \in \mathcal{J} \\ j < k}} \min(t_j^f - t_j^s, t_k^f - t_k^s). \quad (7)$$

The bounded network utilization is then

$$U_g = \frac{T_{\text{overlap}}}{T_{\text{max}}} \in [0, 1]. \quad (8)$$

A higher U_g indicates that more non-local gates are executed simultaneously, reflecting heavier usage of the network's entanglement generation capabilities.

4.5 System Execution-Latency Performance

The Execution-Latency Performance (ELP) of each job quantifies how close its latency is to the ideal execution time:

$$\text{ELP}_j = \frac{T_{j,e}}{T_{j,l}}, \quad (9)$$

where $T_{j,e}$ is the execution time of job j , and the latency $T_{j,l}$ is the sum of the execution time and the waiting time for the job in the queue. The ideal value of $\text{ELP}_j = 1$ indicates that the job is executed without waiting.

The System Execution-Latency Performance (SELP) represents the geometric mean of the proportion of execution time and latency for all the jobs:

$$\text{SELP} = \left(\prod_{j=1}^{|\mathcal{J}|} \text{ELP}_j \right)^{\frac{1}{|\mathcal{J}|}}, \quad (10)$$

where $|\mathcal{J}|$ is the total number of jobs. An ideal $\text{SELP} = 1$ signifies that, on average, all jobs achieve their ideal execution times.

4.6 Fairness Among Jobs

The fairness f metric measures the execution times and latencies among jobs, capturing how equally the schedulers affect them:

$$f = 1 - \sigma(\text{ELP}), \quad (11)$$

where $\sigma(\text{ELP})$ denotes the standard deviation of ELP_j for each DQC job j . An ideal value of $f = 1$ indicates perfect fairness—i.e., all jobs are executed concurrently in the quantum network.

5 Scheduling Methods

As multiple DQC jobs with varying execution times arrive in each time slot, schedulers are designed to determine their concurrency and execution order. Given that scheduling in a parallelized queue is NP-hard, schedulers aim to deliver solutions based on different optimization objectives.

5.1 Resource-Prioritize Scheduler

The Resource-Prioritize Scheduler is designed to maximize the utilization of the total available QPU resources. Its scheduling decisions are guided by two criteria. First, it prioritizes the subsets of the parallelized jobs that maximize node utilization, ensuring that as many nodes as possible are actively engaged at each scheduling step. Second, among subsets achieving the same maximal utilization, it prioritizes the one with the shortest total estimated execution time. The pseudo-code is described in Algorithm 1.

This procedure ensures that the scheduler simultaneously maximizes QPU utilization and minimizes total execution time at each scheduling step, until all DQC jobs in the time slot have been scheduled.

5.2 EPR Scheduler

The EPR Scheduler prioritizes DQC jobs with a smaller number of EPR pairs required. The job queue is ordered in ascending order based on EPR usage, ensuring that jobs requiring fewer non-local entanglement resources are executed earlier, subject to the constraint of available nodes at each step. A lower demand for EPR pairs generally leads to shorter execution times,

Algorithm 1 Resource-Prioritize Scheduler

```
1: Input: arrival job set  $\mathcal{J}$ , nodes  $\mathcal{N}$ 
2: Output: schedule  $\mathcal{S}$ 
3: for all job  $j \in \mathcal{J}$  do
4:   Estimate execution time  $T_j$  and required QPUs  $R_j$ 
5: end for
6: while  $\mathcal{J} \neq \emptyset$  do
7:   best_combo  $\leftarrow \emptyset$ , best_util  $\leftarrow 0$ , best_time  $\leftarrow 0$ 
8:   for all combinations  $C$  of  $\mathcal{J}$  do
9:      $R_{\text{tot}} \leftarrow \sum_{j \in C} R_j$ 
10:    if  $R_{\text{tot}} \leq |\mathcal{N}|$  then
11:       $T_{\text{tot}} \leftarrow \sum_{j \in C} T_j$ 
12:      if  $R_{\text{tot}} > \text{best\_util}$ 
13:        or ( $R_{\text{tot}} = \text{best\_util}$  and  $T_{\text{tot}} < \text{best\_time}$ )
14:        then
15:          best_combo  $\leftarrow C$ 
16:          best_util  $\leftarrow R_{\text{tot}}$ 
17:          best_time  $\leftarrow T_{\text{tot}}$ 
18:        end if
19:      end if
20:    end for
21:    for all job  $j \in \text{best\_combo}$  do
22:      Remove job  $j$  from  $\mathcal{J}$ 
23:    end for
24:  end while
25: return  $\mathcal{S}$ 
```

thereby reducing the waiting time of subsequent jobs in the queue. The pseudo-code is described in Algorithm 2.

In contrast to a Resource-Prioritize Scheduler, which aims to maximize QPU utilization at every scheduling step, the EPR Scheduler focuses on executing low-EPR jobs early rather than saturating node usage. Consequently, the EPR scheduler has low QPU utilization because its priority scheme terminates parallelization whenever a job cannot join the previously selected high-priority jobs, even if subsequent jobs could be accommodated.

5.3 EPR Scheduler with Node Selection

Given that the EPR scheduler has relatively low QPU utilization and considering that the network exhibits heterogeneous link characteristics, the integration of a node-selection algorithm (Algorithm 3) with the EPR scheduler enhances resource allocation by prioritizing nodes that are connected via the most efficient links to reduce job's execution time and improve overall scheduling performance.

5.4 ASAP Scheduler

In the ASAP scheduling method, nodes are released asynchronously as their assigned jobs complete. Rather than waiting for all nodes to become idle at the end of each scheduling step, as the previous two schedulers do,

Algorithm 2 EPR Scheduler

```
1: Input: arrival job set  $\mathcal{J}$ , nodes  $\mathcal{N}$ 
2: Output: schedule  $\mathcal{S}$ 
3: for all job  $j \in \mathcal{J}$  do
4:   Required QPUs  $R_j$ , and EPR usage  $E_j$ 
5: end for
6: Sort  $\mathcal{J}$  in ascending order of  $E_j$ 
7: while  $\mathcal{J} \neq \emptyset$  do
8:   Used node set  $U \leftarrow \emptyset$ 
9:   for all job  $j \in \mathcal{J}$  do
10:    combination  $\mathcal{C} \leftarrow$  nodes not in  $U$ 
11:    if  $|\mathcal{C}| < R_j$  then
12:      continue
13:    end if
14:    Remove job  $j$  from  $\mathcal{J}$ 
15:  end for
16: end while
17: return  $\mathcal{S}$ 
```

Algorithm 3 Node-selection algorithm

```
1: Input: Quantum network graph  $G$  with link weights, select  $\mathcal{K}$  nodes in available nodes  $\mathcal{N}$ 
2: Output: Optimal node group  $N^*$ 
3:  $N^* \leftarrow \text{None}$ 
4: min_weight  $\leftarrow +\infty$ 
5: for all node subsets  $N \subseteq \mathcal{N}$  such that  $|N| = \mathcal{K}$  do
6:   weight  $\leftarrow 0$ 
7:   for all pairs  $(u, v)$  where  $w(u, v)$  is the link weight do
8:     weight  $\leftarrow \text{weight} + w(u, v)$ 
9:   end for
10:  if weight  $< \text{min\_weight}$  then
11:    min_weight  $\leftarrow \text{weight}$ 
12:     $N^* \leftarrow N$ 
13:  end if
14: end for
15: return  $N^*$ 
```

this scheduler continuously monitors job requirements and node availability, allocating newly freed nodes to pending jobs whenever possible. This dynamic reassignment further improves overall resource utilization across the network, as described in Algorithm 4.

Algorithm 4 ASAP Scheduler

```

1: Input: job queue  $Q$ , nodes  $\mathcal{N}$ 
2: Output: schedule  $\mathcal{S}$ 
3: for all  $j \in Q$  do
4:   Estimate execution time  $T_j$  and required QPUs  $R_j$ 
5: end for
6: Initialize  $A[n] \leftarrow 0$  for all  $n \in \mathcal{N}$ ,  $\mathcal{S} \leftarrow \emptyset$ ,  $round \leftarrow 0$ 
7: while  $Q \neq \emptyset$  do
8:    $scheduled\_round \leftarrow \emptyset$ ,  $used\_nodes \leftarrow \emptyset$ 
9:    $round\_start \leftarrow \min_{n \in \mathcal{N}} A[n]$ 
10:  for all  $j \in Q$  do
11:     $candidate\_nodes \leftarrow$  free nodes  $\leq round\_start$ 
    not in  $used\_nodes$ 
12:    if  $|candidate\_nodes| \geq R_j$  then
13:       $assigned\_nodes \leftarrow candidate\_nodes$ 
14:       $finish \leftarrow round\_start + T_j$ 
15:      Record  $(j, assigned\_nodes, round\_start, finish)$ 
      in  $scheduled\_round$ 
16:      for all  $n \in assigned\_nodes$  do
17:         $A[n] \leftarrow finish$ 
18:      end for
19:      Add  $assigned\_nodes$  to  $used\_nodes$ 
20:      Remove  $j$  from  $Q$ 
21:    end if
22:  end for
23: end while
24: return  $\mathcal{S}$ 

```

5.5 PPO Scheduler

The reinforcement learning model, Proximal Policy Optimization (PPO) [18], illustrated in Figure 3, is applied to schedule DQC jobs based on the designed reward functions.

Similar to the other scheduling methods, the environment of the PPO model consists of a set of DQC jobs arriving in each time slot. After receiving these jobs, at each step, the actor of the PPO model attempts to accommodate the jobs until the resource constraints are met. The actor iterates through these steps until all DQC jobs are scheduled for execution, producing the grouped DQC jobs for the environment.

Upon receiving the PPO model’s schedule, job execution times are derived from the dataset generated by Qoala Simulator [19], and individual job latencies are calculated. Using transitions from the rollout buffer, the model trains with a mini-batch size of 64, updating every 1024 transitions. Through gradient descent on

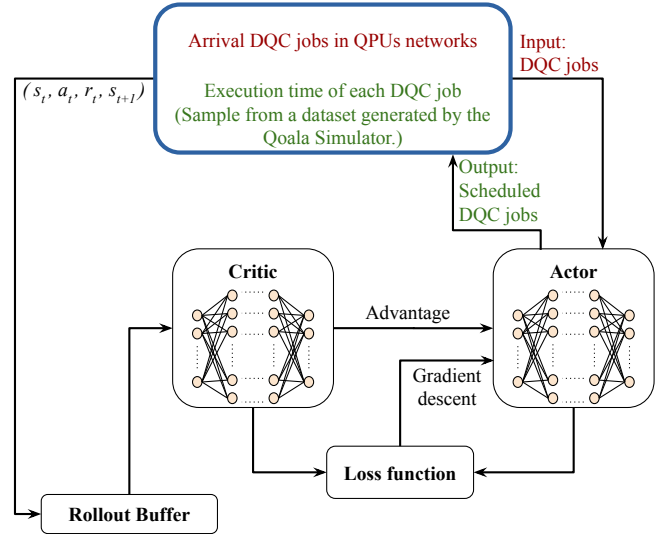


Figure 3: The PPO framework comprises the environment (blue boxed region), fully connected actor and critic networks, the rollout buffer, and the loss function. At each time slot, arriving DQC jobs compose the input state to the actor, and the actor schedules the jobs. Based on the execution order and execution times, rewards are computed. For each job selected at step t , a transition (s_t, a_t, r_t, s_{t+1}) is stored in the rollout buffer, where s_t denotes the state before selecting this job, a_t represents the action taken to select this job, r_t is the reward, and s_{t+1} is the next state after action selection. The critic uses these transitions to estimate the advantage function, guiding the actor toward better performance. The loss function combines the actor’s expected returns and the critic’s value estimates, and is optimized via gradient descent to enhance performance in subsequent time slots.

the loss function and the advantage estimates, the critic improves DQC job selection to maximize rewards.

5.5.1 Input Space

At each step, the input state is represented by a matrix $S \in \mathbb{R}^{|\mathcal{J}| \times 3}$, encoding the features of $|\mathcal{J}|$ DQC jobs. Each row s_j corresponds to job j and its associated features: the number of required QPUs (R_j), EPR pairs (E_j), and the estimated execution time (T_j). Formally, the state matrix is defined as:

$$S = \begin{bmatrix} s_1 \\ s_2 \\ \vdots \\ s_{|\mathcal{J}|} \end{bmatrix} = \begin{bmatrix} R_1 & E_1 & T_1 \\ R_2 & E_2 & T_2 \\ \vdots & \vdots & \vdots \\ R_{|\mathcal{J}|} & E_{|\mathcal{J}|} & T_{|\mathcal{J}|} \end{bmatrix} \quad (12)$$

5.5.2 Action

The model employs a multi-selection action space where the probability of selecting each job j is computed as follows:

$$\pi_\theta(a_j | S) = \frac{\exp(\ell_j)}{\sum_{j=1}^{|\mathcal{J}|} \exp(\ell_j)}, \quad (13)$$

where $\pi_\theta(a_j | S)$ denotes the probability of selecting job j given the current state S under policy π_θ , ℓ_j is the logit produced by the actor for job j . The denominator normalizes the logits using the softmax function to produce a valid probability distribution over all jobs.

The actor selects jobs in decreasing probability order without exceeding the maximum number of available nodes at each step. The selected jobs are executed in parallel. For the remaining jobs, the selection procedure is repeated while masking the jobs that have already been selected in previous steps.

5.5.3 Reward

The goal of the model is to achieve a short makespan while leaving possible spare nodes, allowing further optimization of execution time through a node selection algorithm. This differs from the Resource-Priority and ASAP schedulers, which are designed to keep available nodes occupied most of the time.

Since the number and types of arriving DQC jobs in each time slot are stochastic, directly using the makespan as the reward function is not feasible. Instead, we minimize the latency of each job. Furthermore, an EPR-aware incentive is incorporated.

Normalized latency penalty Let e_j and l_j denote the execution time and latency of job j , respectively. The total latency is

$$L = \sum_{j=1}^{|\mathcal{J}|} l_j. \quad (14)$$

To obtain a scale-invariant metric, L is normalized by the worst-case serialized execution

times in descending order $e_{(1)} \geq \dots \geq e_{(|\mathcal{J}|)}$, we define the latency reward R_{lat} as:

$$R_{\text{lat}} = \frac{L}{L_{\text{max}}}, \quad L_{\text{max}} = \sum_{j=1}^{|\mathcal{J}|} (|\mathcal{J}| - j + 1) e_{(j)} \quad (15)$$

Integrated PPO Reward For a PPO scheduler without node selection, the link quality between QPUs is assumed to be unknown. Let E_j denote the EPR requirement of job j . We define the EPR reward $R_{\text{EPR}}^{(1)}$ as:

$$R_{\text{EPR}}^{(1)} = \frac{1}{|\mathcal{J}|} \sum_m \sum_j \frac{1}{E_j + \gamma D_{m-1}}, \quad (16)$$

with:

$$D_{m-1} = \max_j E_j, \quad D_0 = 0. \quad (17)$$

Here, γ is the coefficient of the previous-step EPR value (D_{m-1}). A larger D_{m-1} increases the denominator and thus reduces the reward. Therefore, to obtain a higher reward from this term, the combined DQC jobs in the earlier step should have the smallest possible maximum EPR pair, minimizing their impact on the later step. This reward term guides the PPO model's behavior similarly to the EPR scheduler, which prioritizes jobs requiring fewer EPR pairs.

The integrated PPO reward is

$$r^{(1)} = -R_{\text{lat}} + \iota^{(1)} R_{\text{EPR}}^{(1)}, \quad (18)$$

where $\iota^{(1)}$ balances the normalized latency penalty with an EPR-aware incentive.

Integrated PPO with Node Selection Reward

Assuming that link quality is known, we could integrate PPO-based model with the node selection algorithm (Algorithm 3).

For parallelized jobs with limited usable nodes, jobs requiring more EPR pairs typically incur longer execution times. Assigning these jobs to higher-quality links while allocating jobs with fewer EPR pairs to lower-quality links can reduce the overall completion time. In contrast, assigning complex jobs to low-quality links would prolong execution and increase the total completion time of the parallelized set.

Therefore, within a parallelized set, higher rewards are assigned when jobs requiring more EPR pairs select higher-quality links than those requiring fewer EPR pairs.

Let o_j denote the node-selection priority for job j , taking values from 0 to $m-1$ in a set of m parallel jobs, with a lower o_j indicating a higher priority for selecting relatively better links. Let β denote the weighting coefficient representing the effect of the link allocation term within a parallelized group. The reward is defined as

$$R_{\text{EPR}}^{(2)} = \frac{1}{|\mathcal{J}|} \sum_m \sum_j \frac{1}{\beta E_j(o_j + 1) + \gamma D_{m-1}}. \quad (19)$$

For a fixed set of DQC jobs and their EPR pair requirements in a parallelized set, minimizing $\sum_j E_j(o_j + 1)$ encourages jobs with larger E_j to select nodes connected by high-quality links with higher priority. When a high-EPR job has higher priority, its node-selection priority o_j is smaller, reducing $E_j(o_j + 1)$. In contrast, scheduling it later increases this term and decreases the reward.

The integrated reward used for PPO with node selection is defined as

$$r^{(2)} = -R_{\text{lat}} + \iota^{(2)} R_{\text{EPR}}^{(2)}, \quad (20)$$

where $\iota^{(2)}$ balances the normalized latency penalty with an EPR-aware incentive.

Summary Both rewards penalize high latency among DQC jobs while prioritizing the scheduling of DQC jobs with fewer EPR pairs. With node selection, $R_{\text{EPR}}^{(2)}$ further encourages DQC jobs with longer expected execution times to utilize higher-quality links among parallelized jobs.

5.5.4 Loss Function

The loss function \mathcal{L} is a weighted sum of the clipped policy loss \mathcal{L}_π , value loss \mathcal{L}_v , and entropy bonus \mathcal{H} , as described in [18]:

$$\mathcal{L} = \mathcal{L}_\pi + c_v \mathcal{L}_v - c_e \mathcal{H}, \quad (21)$$

where c_v and c_e are the coefficients of value loss \mathcal{L}_v and entropy bonus \mathcal{H} , respectively.

5.6 Benchmark Schedulers

Below, we provide a brief explanation of the benchmark schedulers from [8].

5.6.1 FIFO Scheduler

In the FIFO scheduler, jobs are scheduled strictly in the order of arrival, and each job is assigned to execute when a sufficient number of QPU nodes is available.

5.6.2 LIST Scheduler

The LIST scheduler [11] initially follows a FIFO ordering of jobs. However, it enables a job to be scheduled earlier when the required nodes are available, even if its preceding job cannot run in parallel with the already selected jobs, thereby enhancing node utilization and reducing overall waiting time.

5.7 Schedulers Summary

In summary, as shown in Table 1, the scheduling strategies differ in queuing flexibility, node utilization, the parallelized job set end condition, and the update mechanism. FIFO follows a fixed order and has low node

usage, making it simple but unable to group jobs efficiently. LIST introduces flexibility by allowing later jobs to combine, achieving medium node utilization. Resource Priority maximizes node usage by prioritizing a parallelized job set with high node demand and short estimated execution times, offering both order flexibility and high efficiency.

Schedulers based on EPR prioritize jobs requiring fewer EPR pairs. The basic EPR scheduler maintains a fixed execution order that favors low-EPR jobs, while EPR (Node Selection) further improves execution by selecting nodes with better link quality, as some nodes are likely to remain unoccupied in these two scenarios.

Both the PPO and PPO with node selection schedulers schedule DQC jobs using trained PPO models guided by their respective reward functions. Although the reward includes terms encouraging the prioritization of jobs with fewer EPR pairs, it does not enforce a strict ordering as in EPR schedulers. Instead, for both of the PPO-based schedulers, scheduling continues until no nodes are available. Consequently, node utilization is medium, as its tendency to prioritize low-EPR jobs leads to relatively sparse node usage but accommodates jobs until no nodes are available.

Finally, unlike previous scheduling methods that statically generate parallel job sets until all nodes are available, the ASAP scheduler dynamically assigns jobs as nodes become available, keeping free nodes busy whenever they can execute a pending job, achieving flexible scheduling while necessitating continuous monitoring.

6 Simulation Evaluation

Simulations have been developed and executed using the Qoala Simulator, which offers a user-friendly Python API that allows users to mimic both the software and hardware of real quantum network nodes, execute quantum programs, and gather statistics.

6.1 Simulation Settings

In this section, both the specific DQC jobs and the link parameters applied in the simulation are presented.

6.1.1 DQC Jobs

To compare the scheduling algorithms presented in Section 5, we consider several quantum circuits with 5 to 15 qubits. These circuits are of practical interest and are briefly described in Appendix A. The types of these quantum circuits (DQC jobs) include the preparation of GHZ and graph states, as well as the execution of the Quantum Approximate Optimization Algorithm (QAOA), Quantum Fourier Transform (QFT), and Variational Quantum Eigensolver (VQE).

6.1.2 Job Selection Distribution

A set of jobs Γ , comprising all types of quantum circuits, each with sizes ranging from 5 to 15 qubits and used for

Scheduler	Features	Order	Nodes Usage	End Condition	Update
FIFO	Combine in sequence	Fixed	Low	Next job cannot be grouped	End of parallelized job set
LIST	Allow later jobs to combine	Flexible	Medium	No jobs or no available nodes	End of parallelized job set
Resource-Priority	Prioritize jobs with maximum node usage and minimal estimated time	Flexible	High	No jobs or no available nodes	End of parallelized job set
EPR	Prioritize jobs with minimal EPR	Fixed	Low	Next job cannot be grouped	End of parallelized job set
EPR (Node Selection)	Same as EPR but integrated nodes selection	Fixed	Low	Next job cannot be grouped	End of parallelized job set
PPO	Scheduled by trained models with reward Eq. (18)	Flexible	Medium	No jobs or no available nodes	End of parallelized job set
PPO (Node Selection)	Scheduled by trained models with reward Eq. (20)	Flexible	Medium	No jobs or no available nodes	End of parallelized job set
ASAP	Jobs assigned dynamically	Flexible	High	No jobs or no available nodes	When nodes available

Table 1: Summary table of the schedulers.

random selection, is ordered by the number of EPR pairs required, from smallest to largest. In the simulations, both the network load and the job selection probabilities are varied. The latter variation is referred to as the varied job selection distribution.

A non-uniform sampling distribution is imposed over the ordered set of jobs. Each job j is assigned a weight

$$w_j = j^\tau, \quad j = 1, \dots, |\Gamma|, \quad (22)$$

where $\tau \in [0, 1]$ controls the degree of bias. When $\tau = 0$, the distribution is uniform, whereas $\tau = 1$ produces a linear weighting. The sampling probabilities are obtained by normalizing these weights:

$$p_j = \frac{w_j}{\sum_{j=1}^{|\Gamma|} w_j}. \quad (23)$$

As the bias τ in the job selection distribution increases, jobs requiring a larger number of EPR pairs become more likely to be sampled.

6.1.3 Link Parameters

Following the heterogeneous links modeled in Section 3.2.1, and according to [17], the link parameters are summarized in Table 2, where $\eta_{\text{penalty}} = 0.12$ corresponds to a fidelity of 0.88, and $\eta_{\text{penalty}} = 0.20$ corresponds to a fidelity of 0.95. We recall that the fidelity F

quantifies the quality of the generated entangled state relative to an ideal Bell pair, with higher fidelity indicating a state closer to the desired maximally entangled state.

Table 3 summarizes the performance parameters for trapped-ion links, including the calculated success probability P_s , the corresponding fidelity F of the generated entangled pairs, cycle time t_{cycle} , and the state delay t_{state} , which is derived from t_{cycle} and P_s according to Eq. (2).

6.2 Results

Due to the input space (Section 5.5.1) limitation of the proposed PPO-based scheduler, only a fixed number of DQC jobs can arrive per time slot. To mitigate this constraint, multiple models were trained with fixed arrival sizes ranging from 3 to 12, corresponding to the lower and upper bounds of the truncated Poisson arrival model. The simulation results for all schedulers, which process arriving DQC jobs over 1000 time slots, are evaluated using the performance metrics in Section 4.

6.2.1 Makespan

In Table 4 and Table 5, as the network load increases and the selection favors DQC jobs requiring more EPR pairs, the makespan, which is the time required to complete all jobs arriving in the time slot, also increases.

Link quality	$\eta_{FC}^{\text{ion} \rightarrow \text{telecom}}$	$\eta_{\text{det}}^{\text{telecom}}$	η_{penalty}	η_{ion}	α	$d(\text{km})$
Bad	0.5	0.75	0.12	0.87	0.2	0.1
Medium	0.5	0.75	0.20	0.87	0.2	0.1
Good	0.7	0.90	0.20	0.87	0.2	0.1

Table 2: Link parameters for a trapped-ion link at 0.1 km. Parameters are chosen within reasonable ranges as mentioned in [17]

Link quality	t_{cycle} (ns)	P_s	F	t_{state} (ns)
Worst	1.8×10^6	6.37×10^{-3}	0.88	2.83×10^8
Medium	1.0×10^6	1.06×10^{-2}	0.95	9.42×10^7
Good	2.0×10^5	2.99×10^{-2}	0.95	6.67×10^6

Table 3: Performance parameters for trapped-ion links. t_{cycle} for the worst-case link quality is estimated based on the experiments in [20], whereas the lowest t_{cycle} for a high-quality link uses the optimistic laboratory setting in [17].

In Fig. 4, both EPR (node selection) and PPO (node selection) achieve the lowest makespan across varying network loads and job type distributions. This improvement in makespan arises because the node selection algorithm leverages information about heterogeneous network links. Although not all QPUs are fully utilized at every scheduling stage, prioritizing QPUs connected by higher-quality links reduces the time required for entanglement generation and state preparation.

There is a slight performance difference between EPR (node selection) and PPO (node selection) under varying network loads. In Fig. 4a and Fig. 4c, when the network load is 4 (i.e., the number of arriving jobs typically ranges from 3 to 6), the curves of EPR (node selection) and PPO (node selection) almost overlap, indicating that the arriving jobs have similar makespan in most time slots. However, as shown in Fig. 4b and Fig. 4d, when the network load increases to 8 (i.e., the number of arriving jobs typically ranges from 6 to 10), the PPO (node selection) curve is consistently slightly lower than that of EPR (node selection), indicating a higher makespan. This suggests that although PPO (node selection) converges during training, its reward function still requires further improvement, particularly under higher network loads with more incoming jobs.

The scheduler with the second-lowest makespan is the ASAP scheduler. It is designed to allocate QPUs as soon as one of the DQC jobs finishes and free QPUs become available for the remaining jobs. Its mechanism enables more dynamic job selection by utilizing idle QPUs immediately, thereby reducing the makespan.

Among the remaining schedulers, Resource-Priority achieves the third-lowest makespan. EPR, PPO, FIFO, and LIST exhibit largely similar makespan performance; however, the average makespan in LIST is consistently lower than that of FIFO, and PPO is lower than EPR. This is attributed to their higher node utilization, as summarized in Table 1, which enables greater parallelization to shorten the makespan.

6.2.2 QPU Utilization

Figure 5 exhibits the cumulative probability of QPU utilization per time slot under different scheduling methods. As network load increases, the performance differences among the schedulers become more pronounced.

In Table 6, FIFO yields the lowest average QPU utilization, whereas ASAP and Resource-Priority achieve the highest. The high QPU utilization achieved by these two schedulers can be attributed to their scheduling strategies. The ASAP scheduler executes requests immediately when nodes become available, thereby maximizing node usage frequency. In contrast, the Resource-Priority scheduler prioritizes parallel job sets that maximize node utilization.

As the network load increases and DQC jobs become more complex, QPU utilization in Resource-Priority and EPR (node selection) schedulers becomes more evident compared to ASAP. This is because, although ASAP attempts to allocate nodes immediately, it still involves randomness when assigning QPUs to DQC jobs.

Among the remaining schedulers, LIST, EPR, EPR (node selection), PPO, and PPO (node selection) exhibit largely similar QPU utilization. However, PPO consistently achieves slightly higher average QPU utilization than EPR due to their parallelized termination conditions. In contrast, EPR (node selection) shows higher QPU utilization than PPO (node selection).

6.2.3 Non-Local Gate Rate

Non-Local Gate Rate quantifies the overlap in execution times among DQC jobs, which indicates the frequency of usage of non-local gates. A higher overlap in execution time indicates greater reliance on the entanglement for the non-local gate. Therefore, lower values in this evaluation are preferable.

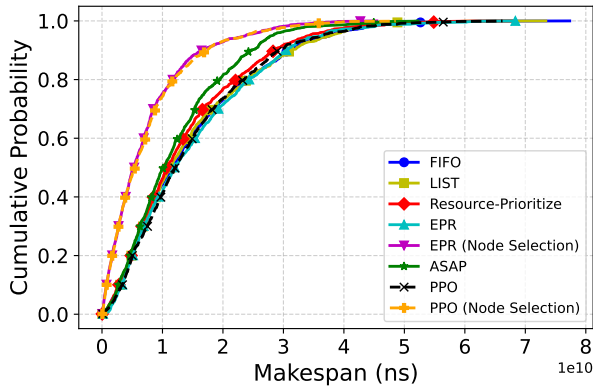
However, in the normalization process, the overlap between every pair of jobs is computed regardless of whether the jobs can actually be parallelized under the constraint of a fixed number of available nodes per step in Eq. (7). Under higher network load, more incoming

Network settings	FIFO	LIST	Resource-Priority	ASAP
$\lambda = 4$	14675060837.24	14583849920.54	13698075533.93	12256971182.37
$\lambda = 4$, bias $\tau = 0.5$	18278432968.54	18156360473.69	17136810859.11	15635403353.12
$\lambda = 8$	25134548598.99	25058603056.68	23637765966.94	20483564744.85
$\lambda = 8$, bias $\tau = 0.5$	31314796010.97	31244654087.13	28554102108.15	25267130550.06

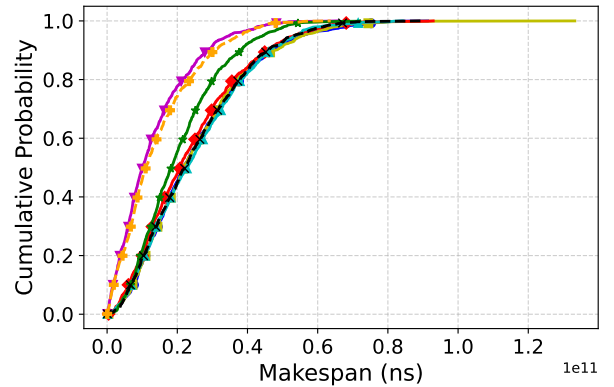
Table 4: Average Makespan (ns) under different network settings.

Network settings	EPR	EPR (Node Selection)	PPO	PPO (Node Selection)
$\lambda = 4$	15011989810.68	7398918761.67	14742636818.89	7585403303.24
$\lambda = 4$, bias $\tau = 0.5$	19393742087.45	9448022638.33	18567995715.54	9576079769.57
$\lambda = 8$	25078153924.57	13122980997.98	24646493381.38	14219413472.53
$\lambda = 8$, bias $\tau = 0.5$	31430545308.44	16846808075.69	30338145199.66	17966769662.61

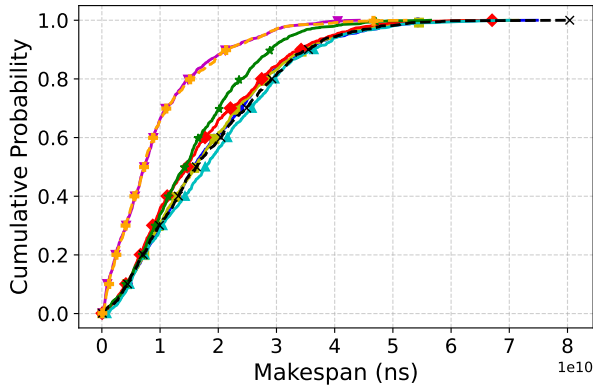
Table 5: Average Makespan (ns) under different network settings.



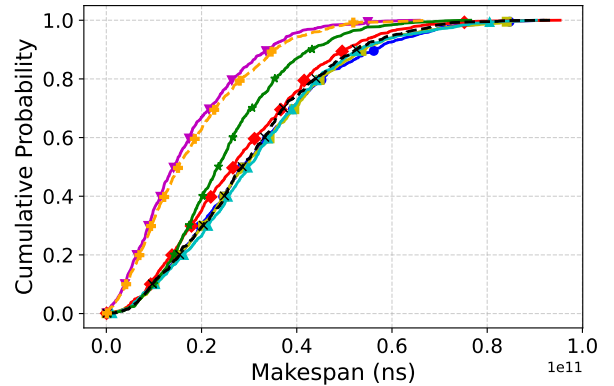
(a) Network load $\lambda = 4$.



(b) Network load $\lambda = 8$.



(c) Network load $\lambda = 4$, with biased parameter $\alpha = 0.5$ for the job selection.

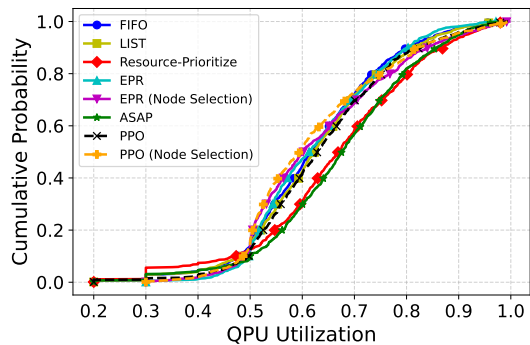


(d) Network load $\lambda = 8$, with biased parameter $\alpha = 0.5$ for the job selection.

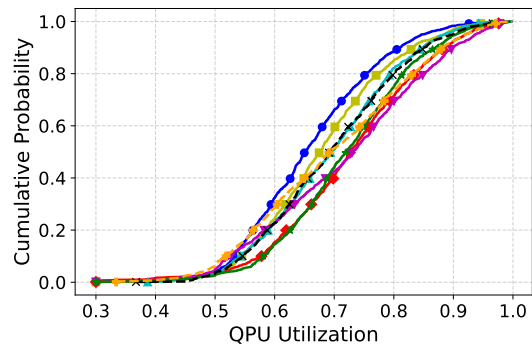
Figure 4: The cumulative probability of makespan in each time slot among different schedulers.

Network settings	FIFO	LIST	Resource-Priority	EPR	EPR (Node Selection)	PPO	PPO (Node Selection)	ASAP
$\lambda = 4$	0.6239	0.6297	0.6641	0.6285	0.6334	0.6396	0.6232	0.6720
$\lambda = 4$, bias $\tau = 0.5$	0.6445	0.6510	0.6702	0.6364	0.6521	0.6457	0.6439	0.6909
$\lambda = 8$	0.6608	0.6818	0.7252	0.6944	0.7194	0.6962	0.6978	0.7204
$\lambda = 8$, bias $\tau = 0.5$	0.6763	0.6968	0.7546	0.7122	0.7388	0.7140	0.7283	0.7388

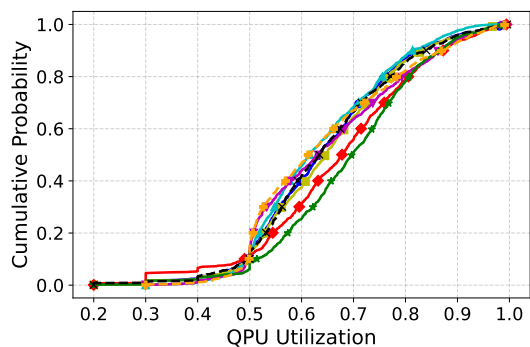
Table 6: Average QPU utilization under different network settings.



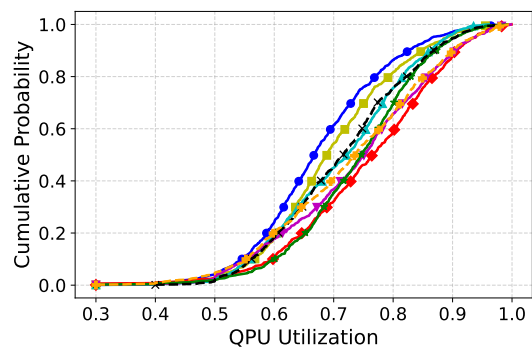
(a) Network load $\lambda = 4$.



(b) Network load $\lambda = 8$.



(c) Network load $\lambda = 4$, with biased parameter $\alpha = 0.5$ for the job selection.



(d) Network load $\lambda = 8$, with biased parameter $\alpha = 0.5$ for the job selection.

Figure 5: The cumulative probability of QPU utilization in each time slot among different schedulers.

jobs cannot be parallelized within the same group. Consequently, jobs from different groups have no real overlap but still contribute to the normalization term.

Similarly, for a given type of quantum circuit, the number of required EPR pairs increases with circuit size, occupying more nodes and forming more parallelized groups, which, in turn, increases the normalization term. As a result, the Non-Local Gate Rate decreases as network load increases and becomes biased toward jobs requiring more EPR pairs, as shown in Table 7. Therefore, only comparisons between schedulers under the same network conditions (i.e., within each row) remain meaningful.

When only a few DQC jobs arrive in a time slot, they may all be parallelized, producing complete overlap and a Non-Local Gate Rate of 1, as shown in Fig. 6. This effect is particularly evident when the network load is 4 in Fig. 6a and Fig. 6c.

With network load 4, the EPR scheduler yields the lowest Non-Local Gate Rate because it strictly groups jobs by EPR pair requirements. As the number of arriving jobs increases, this constraint becomes less influential since a larger number of jobs increases the likelihood that the next jobs can join previously selected jobs for parallelization. When the network load is 8, the FIFO scheduler exhibits the lowest Non-Local Gate Rate, as strict request ordering leads to sparse DQC job distributions when grouping. The LIST scheduler consistently produces a slightly higher Non-Local Gate Rate than FIFO.

Among the remaining schedulers, Resource-Priority and ASAP achieve the highest rates when the network load is 4. When the load increases to 8, the highest values are produced by EPR (Node Selection) and PPO (Node Selection). Under low network load, strategies that utilize more nodes or constantly use the available nodes increase job overlap. However, under higher network load with multiple job groups, EPR (Node Selection) and PPO (Node Selection) tend to schedule jobs with similar execution times within groups, resulting in larger total overlap compared with other schedulers.

6.2.4 System Execution-Latency Performance and Fairness

Unlike previous evaluations of Makespan, QPU utilization, and Non-Local Gate Rate, which quantify the overall performance of arriving DQC job sets, the System Execution-Latency Performance (SELP) and Fairness metrics assess the performance of individual DQC jobs within the queue arranged by the schedulers.

The Execution-Latency Performance (ELP) measures a job’s actual execution time relative to its latency. Values closer to 1 indicate shorter waiting times. Fairness is defined with an upper bound of 1, adjusted by subtracting the standard deviation of the ELP values for all jobs. The optimal value is therefore 1, which corresponds to

minimal variation in ELP among jobs.

However, due to the limited number of QPUs in the network, not all DQC jobs can be executed in parallel. Therefore, both SELP and fairness among jobs are important, with higher values indicating better performance.

Both the EPR scheduler and the EPR (node selection) achieve the highest SELP and fairness in Fig. 7 and Fig. 8. This is because they prioritize jobs with shorter execution times and assign them to high-quality links, thereby avoiding prolonged execution that would result from scheduling on lower-quality links. The PPO scheduler and PPO (node selection) exhibit the next best performance.

The third-best performance is observed with the Resource Priority scheduler in Table 8 and Table 9, particularly under high network load, which achieves relatively high SELP and fairness compared to the other schedulers. This is due to its strategy of compacting as many jobs as possible while prioritizing combinations that consume fewer EPR pairs, resulting in relatively similar execution times and reduced waiting time for the remaining jobs.

It is important to note that the SELP and fairness of the ASAP scheduler exhibit variability similar to benchmark methods such as LIST and FIFO. This is expected, as ASAP is designed solely to dynamically utilize spare QPUs rather than optimize execution-latency performance or fairness.

7 Conclusion

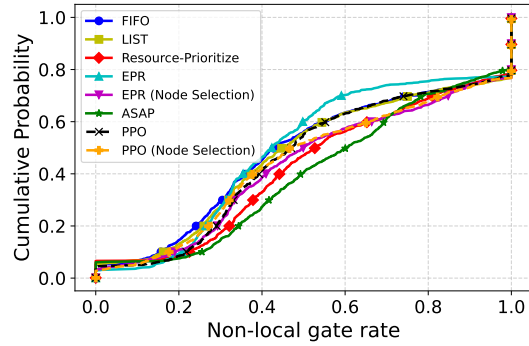
This paper presents an integrated workflow comprising a quantum compiler for compiling distributed quantum computation (DQC) jobs from quantum circuits, an Execution Manager for scheduling DQC jobs, and execution on the Qoala Simulator. As a key contribution, we propose multiple scheduling strategies within the Execution Manager to manage incoming DQC jobs, which are subsequently evaluated using various performance metrics.

The simulation results indicate that different schedulers exhibit distinct advantages. The EPR (node selection) and PPO (node selection) achieve the lowest makespan. The ASAP scheduler performs second best in terms of makespan, while the Resource-Prioritize scheduler achieves the highest QPU utilization. The EPR scheduler achieves the best performance in system execution-latency and fairness. Unlike classical schedulers, the PPO-based schedulers are driven by a reward function, providing greater flexibility.

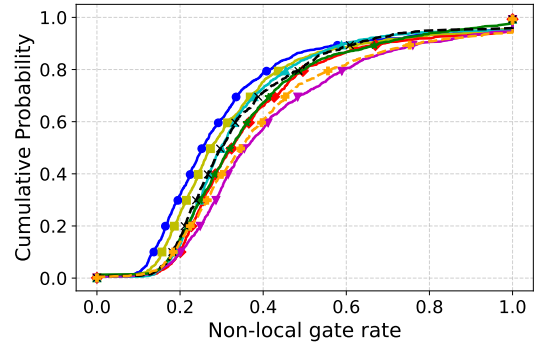
In future work, additional reward strategies could be investigated to further shape the behavior of PPO schedulers, with the aim of optimizing their intended objective (i.e., reducing the makespan, which is the primary goal of this paper). Moreover, the analysis of quantum net-

Network settings	FIFO	LIST	Resource-Priority	EPR	EPR (Node Selection)	PPO	PPO (Node Selection)	ASAP
$\lambda = 4$	0.5297	0.5373	0.5827	0.5163	0.5731	0.5507	0.5622	0.6053
$\lambda = 4$, bias $\tau = 0.5$	0.4884	0.4961	0.5313	0.4538	0.5274	0.4881	0.5149	0.5524
$\lambda = 8$	0.3210	0.3442	0.3892	0.3597	0.4283	0.3604	0.4104	0.3761
$\lambda = 8$, bias $\tau = 0.5$	0.2955	0.3096	0.3586	0.3239	0.3831	0.3276	0.3762	0.3292

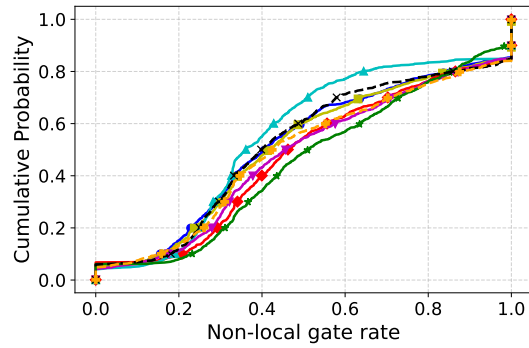
Table 7: Average non-local gate rate under different network settings.



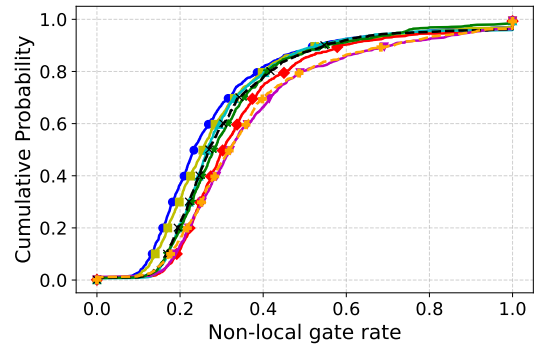
(a) Network load $\lambda = 4$.



(b) Network load $\lambda = 8$.



(c) Network load $\lambda = 4$, with biased parameter $\alpha = 0.5$ for the job selection.



(d) Network load $\lambda = 8$, with biased parameter $\alpha = 0.5$ for the job selection.

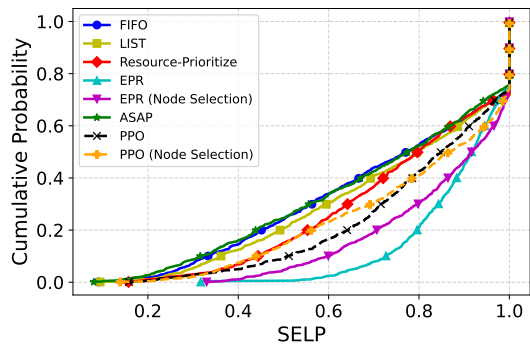
Figure 6: The cumulative probability of non-local gate rate in each time slot among different schedulers.

Network settings	FIFO	LIST	Resource-Priority	EPR	EPR (Node Selection)	PPO	PPO (Node Selection)	ASAP
$\lambda = 4$	0.7233	0.7425	0.7634	0.8872	0.8547	0.8029	0.7926	0.7177
$\lambda = 4$, bias $\tau = 0.5$	0.6892	0.7044	0.7332	0.8697	0.8245	0.7600	0.7752	0.6697
$\lambda = 8$	0.4681	0.5051	0.6534	0.7516	0.7251	0.7118	0.6336	0.4527
$\lambda = 8$, bias $\tau = 0.5$	0.4787	0.5046	0.6276	0.7311	0.6946	0.6865	0.5960	0.4457

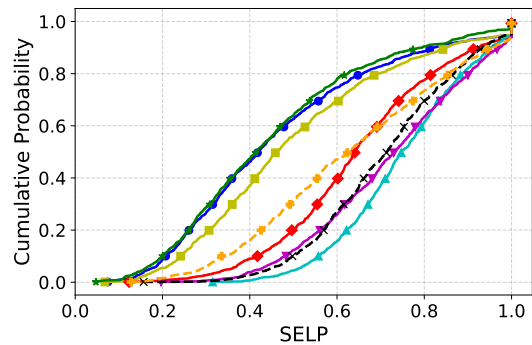
Table 8: Average SELP under different network settings.

Network settings	FIFO	LIST	Resource-Priority	EPR	EPR (Node Selection)	PPO	PPO (Node Selection)	ASAP
$\lambda = 4$	0.7889	0.7964	0.7994	0.8872	0.8616	0.8261	0.8248	0.7854
$\lambda = 4$, bias $\tau = 0.5$	0.7610	0.7669	0.7783	0.8748	0.8394	0.7971	0.8139	0.7497
$\lambda = 8$	0.6818	0.6870	0.7412	0.8064	0.7772	0.7784	0.7343	0.6707
$\lambda = 8$, bias $\tau = 0.5$	0.6867	0.6895	0.7335	0.8024	0.7672	0.7718	0.7213	0.6735

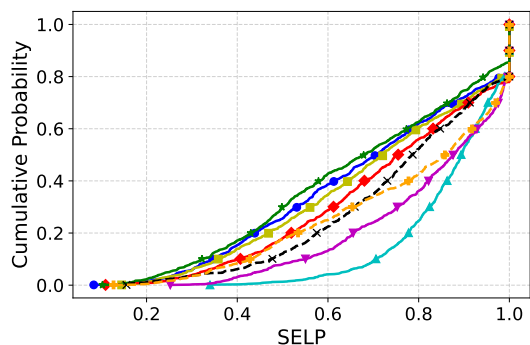
Table 9: Average Fairness under different network settings.



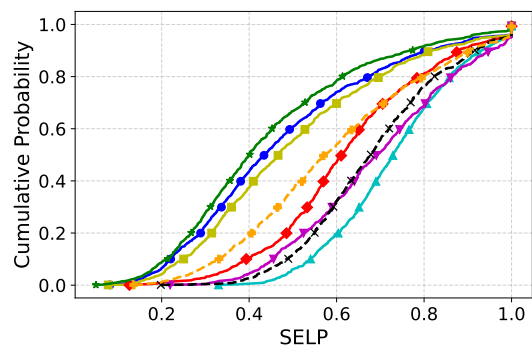
(a) Network load $\lambda = 4$.



(b) Network load $\lambda = 8$.

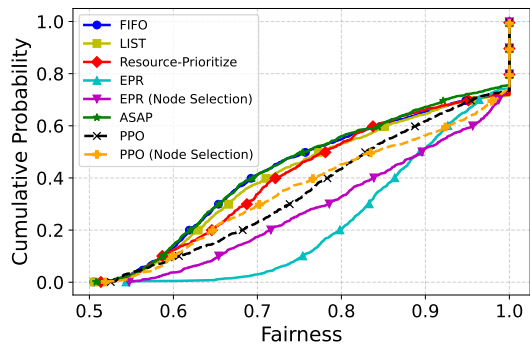


(c) Network load $\lambda = 4$, with biased parameter $\alpha = 0.5$ for the job selection.

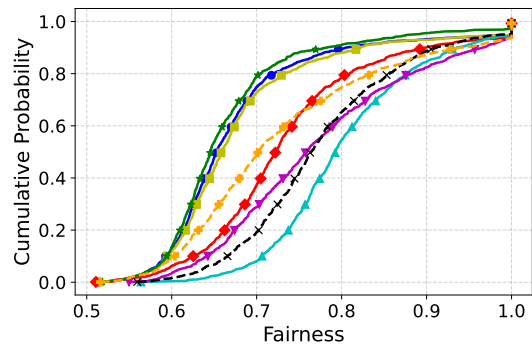


(d) Network load $\lambda = 8$, with biased parameter $\alpha = 0.5$ for the job selection.

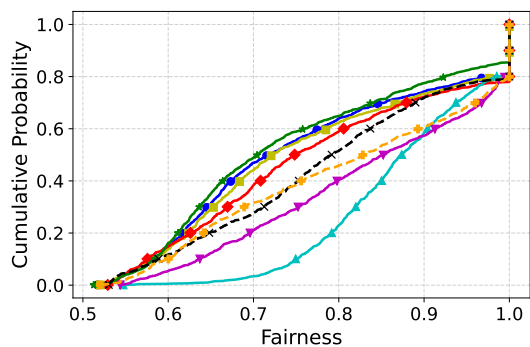
Figure 7: The cumulative probability of SELP in each time slot among different schedulers.



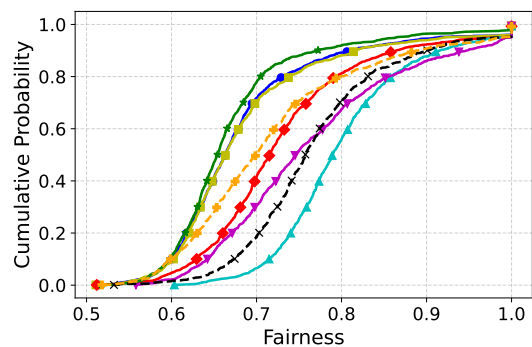
(a) Network load $\lambda = 4$.



(b) Network load $\lambda = 8$.



(c) Network load $\lambda = 4$, with biased parameter $\alpha = 0.5$ for the job selection.



(d) Network load $\lambda = 8$, with biased parameter $\alpha = 0.5$ for the job selection.

Figure 8: The cumulative probability of fairness in each time slot among different schedulers.

work connectivity and topology, along with their effects on scheduling strategies, could be further investigated. In addition, with the advancement of quantum computers and their entanglement-based connections, DQC job schedulers on realistically connected quantum computer networks could be further evaluated and optimized.

Data Availability

All data and code required to reproduce all plots shown herein are available at <https://doi.org/10.5281/zenodo.18802412>.

Acknowledgements

This work was financially supported by the European Union’s Horizon Europe research and innovation program under grant agreement No. 101102140 – QIA Phase 1, and by Research Ireland under Grant number 13/RC/2077.P2. Furthermore, this work benefited from the High Performance Computing facility at the University of Parma, Italy.

References

- [1] Angela Sara Cacciapuoti, Marcello Caleffi, Francesco Tafuri, Francesco Saverio Cataliotti, Stefano Gherardini, and Giuseppe Bianchi. Quantum internet: Networking challenges in distributed quantum computing. *IEEE Network*, 34(1):137–143, 2019.
- [2] Nicolas Brunner, Daniel Cavalcanti, Stefano Pironio, Valerio Scarani, and Stephanie Wehner. Bell nonlocality. *Rev. Mod. Phys.*, 86:419–478, Apr 2014.
- [3] Michele Amoretti and Stefano Carretta. Entanglement verification in quantum networks with tampered nodes. *IEEE Journal on Selected Areas in Communications*, 38(3):598–604, 2020.
- [4] Marcello Caleffi, Michele Amoretti, Davide Ferrari, Jessica Illiano, Antonio Manzalini, and Angela Sara Cacciapuoti. Distributed quantum computing: a survey. *Computer Networks*, 254:110672, 2024.
- [5] Davide Ferrari, Stefano Carretta, and Michele Amoretti. A modular quantum compilation framework for distributed quantum computing. *IEEE Transactions on Quantum Engineering*, 4:1–13, 2023.
- [6] Xu Xu, Yu Liu, Yingling Mao, and Yuanyuan Yang. Remote gate scheduling in distributed quantum computing. In *2025 IEEE 45th International Conference on Distributed Computing Systems (ICDCS)*, pages 846–856. IEEE, 2025.
- [7] Daniele Cuomo, Marcello Caleffi, Kevin Krsulich, Filippo Tramonto, Gabriele Agliardi, Enrico Prati, and Angela Sara Cacciapuoti. Optimized compiler for distributed quantum computing. *ACM Transactions on Quantum Computing*, 4(2):1–29, 2023.
- [8] Davide Ferrari, Michele Bandini, and Michele Amoretti. Execution management of distributed quantum computing jobs. In *2024 IEEE International Conference on Quantum Computing and Engineering (QCE)*, volume 2, pages 150–154. IEEE, 2024.
- [9] Stephen DiAdamo, Marco Ghibaudi, and James Cruise. Distributed quantum computing and network control for accelerated vqe. *IEEE Transactions on Quantum Engineering*, 2:1–21, 2021.
- [10] Rhea Parekh, Andrea Ricciardi, Ahmed Darwish, and Stephen DiAdamo. Quantum algorithms and simulation for parallel and distributed quantum computing. In *2021 IEEE/ACM Second International Workshop on Quantum Computing Software (QCS)*, pages 9–19. IEEE, 2021.
- [11] Berit Johannes. Scheduling parallel jobs to minimize the makespan. *Journal of Scheduling*, 9(5):433–452, 2006.
- [12] Richard A Dutton, Weizhen Mao, Jie Chen, and William Watson. Parallel job scheduling with overhead: A benchmark study. In *2008 international conference on networking, architecture, and storage*, pages 326–333. IEEE, 2008.
- [13] Jiří Sgall and Gerhard J Woeginger. Multiprocessor jobs, preemptive schedules, and one-competitive online algorithms. In *International Workshop on Approximation and Online Algorithms*, pages 236–247. Springer, 2014.
- [14] Michael Isard, Vijayan Prabhakaran, Jon Currey, Udi Wieder, Kunal Talwar, and Andrew Goldberg. Quincy: fair scheduling for distributed computing clusters. In *Proceedings of the ACM SIGOPS 22nd symposium on Operating systems principles*, pages 261–276, 2009.
- [15] Nitish K Chandra, Eneet Kaur, and Kaushik P Shadreesan. Network operations scheduling for distributed quantum computing. In *2024 IEEE 6th International Conference on Trust, Privacy and Security in Intelligent Systems, and Applications (TPS-ISA)*, pages 506–515. IEEE, 2024.
- [16] Aaron Orenstein and Vipin Chaudhary. Qgroup: Parallel quantum job scheduling using dynamic programming. In *2024 IEEE International conference on quantum computing and engineering (QCE)*, volume 1, pages 990–999. IEEE, 2024.

- [17] Samuel Oslovich, Bart van der Vecht, and Stephanie Wehner. Compilation strategies for quantum network programs using qoala. *arXiv preprint arXiv:2505.06162*, 2025.
- [18] John Schulman, Filip Wolski, Prafulla Dhariwal, Alec Radford, and Oleg Klimov. Proximal policy optimization algorithms. *arXiv preprint arXiv:1707.06347*, 2017.
- [19] Bart van der Vecht, Atak Talay Yücel, Hana Jirovská, and Stephanie Wehner. Qoala: an application execution environment for quantum internet nodes. *arXiv preprint arXiv:2502.17296*, 2025.
- [20] V. Krutyanskiy, M. Galli, V. Krcmarsky, S. Baier, D. A. Fioretto, Y. Pu, A. Mazloom, P. Sekatski, M. Canteri, M. Teller, J. Schupp, J. Bate, M. Meraner, N. Sangouard, B. P. Lanyon, and T. E. Northup. Entanglement of trapped-ion qubits separated by 230 meters. *Phys. Rev. Lett.*, 130:050803, Feb 2023.
- [21] Adetokunbo Adedoyin, John Ambrosiano, Petr Anisimov, William Casper, Gopinath Chennupati, Carleton Coffrin, Hristo Djidjev, David Gunter, Satish Karra, Nathan Lemons, et al. Quantum algorithm implementations for beginners. *arXiv preprint arXiv:1804.03719*, 2018.

A Specific DQC job types

A.1 GHZ State

The Greenberger–Horne–Zeilinger (GHZ) state is an entangled multi-qubit state of the form:

$$|\text{GHZ}_n\rangle = \frac{|0\rangle^{\otimes n} + |1\rangle^{\otimes n}}{\sqrt{2}}. \quad (24)$$

It can be prepared on n qubits by first applying a Hadamard gate to the first qubit, followed by a sequence of CNOT gates connecting the first qubit to all subsequent qubits:

$$|\text{GHZ}_n\rangle = \text{CNOT}_{1,2} \cdots \text{CNOT}_{1,n} H_1 |0\rangle^{\otimes n}. \quad (25)$$

A 5-qubit GHZ circuit using CNOT gates is illustrated schematically in Fig. 9.

A.2 Graph State

A ring graph state associated with a graph $G(V, E)$ is defined as

$$|G\rangle = \left(\prod_{(i,j) \in E} CZ_{i,j} \right) |+\rangle^{\otimes n}, \quad (26)$$

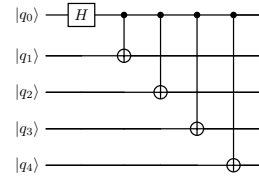


Figure 9: 5-qubit GHZ state preparation. The first qubit is put into superposition via a Hadamard gate, and subsequent qubits are entangled via controlled-NOT operations.

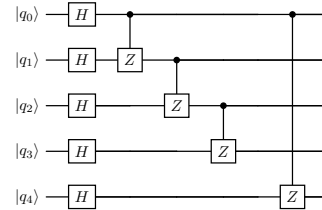


Figure 10: 5-qubit graph state preparation. Each qubit is initialized in the $|+\rangle$ state via a Hadamard gate, and controlled-Z (CZ) gates is introduced according to the edges of the graph.

where $n = |V|$ is the number of vertices. Each qubit is initialized in the $|+\rangle$ state via Hadamard gates, after which entangling controlled-Z operations are applied for every edge $(i, j) \in E$. The quantum circuit is shown in Fig. 10.

A.3 Quantum Approximate Optimization Algorithm (QAOA)

This algorithm is designed to provide approximate solutions to combinatorial optimization problems [21]. It includes the cost Hamiltonian $\hat{H}_c = \sum_{\alpha} C_{\alpha}$, where C_{α} is the quantum clause Hamiltonian, and a mixer Hamiltonian $\hat{H}_b = \sum_j X_j$, where X_j denotes the Pauli- X operator acting on qubit j .

Given a number of rounds $r \geq 1$ and parameter sets $\{\beta_k\}_{k=1}^r$ and $\{\gamma_k\}_{k=1}^r$, the algorithm starts in the uniform superposition $|+\rangle^{\otimes n}$ and alternates the application of the cost and mixer unitaries:

$$U_C(\gamma_k) = e^{-i\gamma_k \hat{H}_c}, \quad (27)$$

$$U_B(\beta_k) = e^{-i\beta_k \hat{H}_b}. \quad (28)$$

This produces the variational state $|\beta, \gamma\rangle$, from which candidate solutions are sampled. The quality of these solutions depends on the chosen round r and the parameters β, γ .

For the MaxCut problem, the cost Hamiltonian $\hat{H}_c = \sum_{(i,j) \in E} \frac{1}{2}(I - Z_i Z_j)$. An illustrative QAOA circuit for a 5-qubit system on the simple ring graph with edges $(0, 1)$, $(1, 2)$, $(2, 3)$, $(3, 4)$, and $(0, 4)$ is shown in Fig. 11.

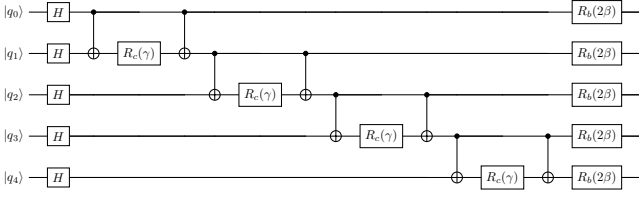


Figure 11: 5-qubit QAOA circuit with one repetition. The cost unitary $U_C(\gamma)$ is implemented via two controlled-NOT and one $R_c(\gamma)$ gates, which is a rotation that depends on the parity of the two qubits. The mixer unitary $U_B(\beta)$ is applied as $R_b(2\beta)$ rotations on all qubits.

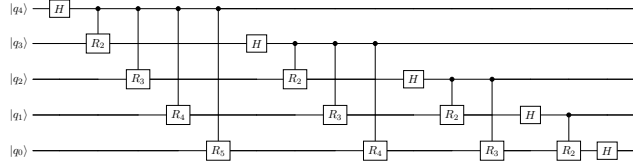


Figure 12: 5-qubit QFT circuit with controlled-phase rotations R_k . Hadamard gates initialize superpositions, and controlled-phase gates implement the Fourier transform phases.

Specifically, the rotation gates applied in the quantum circuit are defined as:

$$R_c(\gamma) = \begin{pmatrix} 1 & 0 \\ 0 & e^{-i\gamma} \end{pmatrix}, \quad (29)$$

$$R_b(\theta, \phi, 2\beta) = \begin{pmatrix} \cos(\theta/2) & -e^{2i\beta} \sin(\theta/2) \\ e^{i\phi} \sin(\theta/2) & e^{i(2\beta+\phi)} \cos(\theta/2) \end{pmatrix}. \quad (30)$$

A.4 Quantum Fourier Transform (QFT)

The Quantum Fourier Transform is defined as:

$$\text{QFT} |x\rangle = \frac{1}{\sqrt{2^m}} \sum_{y=0}^{2^m-1} e^{2\pi i xy/2^m} |y\rangle, \quad (31)$$

where the amplitudes associated with the $|y\rangle$ vectors are the discrete Fourier transforms of the amplitudes of the $|x\rangle$ vectors.

The QFT is implemented recursively, starting with a Hadamard gate applied to the first qubit to create a superposition. Each subsequent qubit is then rotated conditionally using controlled rotations $R_m = \begin{pmatrix} 1 & 0 \\ 0 & e^{2\pi i/2^m} \end{pmatrix}$ on the target qubit. A schematic 5-qubit QFT circuit is shown in Fig. 12.

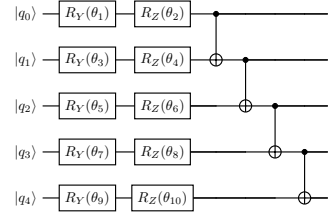


Figure 13: 5-qubit VQE circuit using linear nearest-neighbor entanglement with one repetition. Each qubit undergoes parameterized R_Y and R_Z rotations, followed by controlled-NOT gates between nearest neighbors. The rotation parameters θ_i are randomly initialized in $[0, 2\pi]$.

A.5 Variational Quantum Eigen-solver (VQE)

This is a hybrid quantum-classical algorithm designed to approximate the ground state energy of a given Hamiltonian \hat{H} , as described in Ref. [21]. A variational state $|\psi(\theta_i)\rangle$ is prepared with parameters θ_i , chosen such that the number of parameters scales linearly with the system size. The expectation value of the Hamiltonian is calculated on a quantum computer as

$$E = \frac{\langle \psi(\theta) | \hat{H} | \psi(\theta) \rangle}{\langle \psi(\theta) | \psi(\theta) \rangle}. \quad (32)$$

The parameters θ_i are updated using a classical non-linear optimizer. In this paper, EfficientSU2 is used, for which each qubit is first rotated using parameterized R_Y and R_Z gates with parameters randomly initialized in $[0, 2\pi]$. Entanglement is applied linearly, such that controlled-NOT gates connect each qubit to its nearest neighbor sequentially. A schematic representation of a single-layer 5-qubit VQE is shown in Fig. 13.